BNL-64939

NICKEL HYDROXIDES

James McBreen
Department of Applied Science
Brookhaven National Laboratory
Upton, NY 11973

A chapter prepared for a book "Handbook of Battery Materials", J. O. Besenhard, Editor and VCH, Publisher.

October 1997

1. Introduction

Nickel hydroxides have been used as the active material in the positive electrodes of several alkaline batteries for over a century [1]. These materials continue to attract a lot of attention because of the commercial importance of nickel-cadmium and nickel-metal hydride batteries. In addition to being the cathode active material in nickel metal hydride batteries $Ni(OH)_2$ is an important corrosion product of the anode during cycling. There are several reviews of work in the field [2-10]. Progress in understanding the reactions of nickel hydroxide electrodes has been very slow because of the complex nature of the reactions. Items which are normally trivial exercises for most battery electrodes, such as the determination of the open circuit potential, the overall reaction, and the oxidation state of the charged material, have required much effort and ingenuity. The materials have been studied by an enormous array of spectroscopic, structural and electrochemical techniques. The most significant advance in the understanding of the overall reaction was made by Bode and his co-workers [11]. They established that both the discharged material ($Ni(OH)_2$) and the charged material (NiOOH) could exist in two forms. One form of $Ni(OH)_2$, which was designated as β-$Ni(OH)_2$, is anhydrous and has a layered brucite ($Mg(OH)_2$) structure. The other form, α-$Ni(OH)_2$, is hydrated and has intercalated water between brucite like layers. Oxidation of β-$Ni(OH)_2$ on charge produces β-NiOOH and oxidation of α-$Ni(OH)_2$ produces γ-NiOOH. Discharge of β-NiOOH yields β-$Ni(OH)_2$ and discharge of γ-NiOOH yields α-$Ni(OH)_2$. On discharged stand the α-$Ni(OH)_2$ can dehydrate and recrystallize in the concentrated alkaline electrolyte to form β-$Ni(OH)_2$. They also found that and that β-NiOOH could be converted to γ-NiOOH when the electrode is overcharged. Their overall reaction scheme is shown schematically in Fig. 1. All subsequent work has in general validated these conclusions. The two reaction schemes are often referred to as the β/β and the α/γ cycles.

This review gives a brief overview of the structure of nickel hydroxide battery electrodes and a more detailed review of the solid state chemistry and electrochemistry of the electrode materials. Emphasis is on work done since 1989.

2. Nickel Hydroxide Battery Electrodes

Conventional nickel hydroxide battery electrodes are designed to operate on the β/β cycle, to accommodate the volume changes that occur during cycling, and to have adequate electronic conductivity to yield high utilization of the active material on discharge. The β/β cycle is preferred because there is less swelling of the active material on cycling. The conductivity of β-NiOOH is more than five orders of magnitude higher than that for $Ni(OH)_2$ [12]. As a result there is usually no problem in charging the electrode because the NiOOH that forms increases the conductivity of the active material. However, on discharge the charged material can become isolated in a resistive matrix of the discharged product and cannot be discharged at useful rates [13]. Operation on the β/β cycle is ensured by control of the electrolyte composition and the use of a combination of additives such as Co and Zn. Provisions have to be made for electronic conduction to the active material and confinement of the active material on cycling. Over the years several electrode designs have been used. These include

incorporation of the active material in pocket plates, perforated metal tubes, sintered nickel plaques , plastic bonded electrodes with graphite as the conductive diluent, nickel foams, and fibrous nickel mats.

Pocket and tubular electrodes have been described in detail by Falk and Salkind [1]. McBreen has reviewed work on both sintered plate and plastic bonded electrode technology [9]. More recent work is on the use of nickel foams and nickel mats.

Early work on the use of foams and mats has been reviewed [9]. Nickel fiber, nickel plated steel fiber or nickel plated graphite fiber mats are preferred because they have smaller pores (~50μ) [14]. The most recently developed mats can have porosities as high as 95% [13], and are much lighter than the sintered nickel plaques which typically have porosities between 80% and 90%. Initially standard cathodic impregnation methods were used to load the active material into the foam [9]. More recently the preferred method is to incorporate the $Ni(OH)_2$ in the form of a slurry into the mat [13,14]. This has been called the "suspension impregnation method" [14]. Considerable improvement in the $Ni(OH)_2$ is achieved by the addition of divalent Co compounds to the slurry. The best results were achieved with the addition of 10% CoO [13,15]. The following mechanism has been proposed for this improvement [13]. In the alkaline electrolyte CoO dissolves to form the blue cobaltite ion. The ion precipitates on the $Ni(OH)_2$ particles to form insoluble β-$Co(OH)_2$. On charge the β-$Co(OH)_2$ is oxidized to a highly conductive β-CoOOH which is not reduced on subsequent discharges. The β-CoOOH provides interparticle contact and access of electrons to the active material.

Considerable increases in the capacity density of the electrodes have been achieved through the use of high density β-$Ni(OH)_2$ with a uniform particle size, narrow range of pore sizes, and a high tapping density (1.9-2.0 g/cm^3) [15,16]. Conventional β-$Ni(OH)_2$ consists of irregular particles with 30% inner pore volume, a large range of pore sizes, and a tapping density of ~1.6 g/cm^3. With the new material it is possible to increase the active material filling by 20%. Using this material it was possible to make electrodes with capacity densities exceeding 550 mAh/cm^3. Conventional sintered plates have capacity densities of ~400 mAh/cm^3.

A major problem with pasted plastic bonded and fiber mat electrodes is swelling of the electrode on cycling. This is due to the formation of γ-NiOOH. This causes comminution of the active material and an increase on the pore volume. This problem can be largely avoided by the use of β-$Ni(OH)_2$ containing ~7% of either co-precipitated Cd or Zn. The co-precipitation of one of these additives along with 7% Co also greatly improves the charge acceptance of the electrode at elevated temperatures (up to 45 °C) [15]. This additive combination also greatly improves the charge retention at elevated temperatures [15]. Zinc is preferred over Cd as an additive because of its lower toxicity, and the detrimental effect of Cd on metal hydride electrodes. These advances in the nickel hydroxide electrode represent considerable progress, and have increased the capacity of sealed nickel-cadmium AA cells, at the C rate, from 500 mAh to 800 mAh [15].

3. Solid State Chemistry of Nickel Hydroxides

3.1 Hydrous Nickel Oxides

β-$Ni(OH)_2$, α-$Ni(OH)_2$, β-NiOOH and γ-NiOOH are considered to be the model divalent and trivalent materials for the nickel hydroxide electrode.

3.1.1 β-$Ni(OH)_2$

β-$Ni(OH)_2$ can be made with a well defined crystalline structure and is in many ways similar to the active material in chemically prepared battery electrodes that are made by the method described by Fleischer [17]. Several methods of preparation have been reported. One is to precipitate the hydroxide at 100°C from a nickel nitrate solution by addition of a KOH solution. Further enhancement in the crystallinity of this material has been obtained by hydrothermal treatment in an aqueous slurry containing NH_4OH, KOH [18] or NaOH [19]. A method which produces good crystals has been described by Fievet and Figlarz [20]. The hydroxide is prepared in two steps. First an ammonia solution is added to a nickel nitrate solution at room temperature. The precipitate is washed, and then hydrothermally treated at 200°C. Another method is to precipitate the hydroxide by dropwise addition of 3M $Ni(NO_3)_2$ to hot (90°C) 7M KOH with constant stirring. The precipitate is washed and dried. The $Ni(OH)_2$ is then dissolved in 8M NH_4OH and the resulting blue solution $Ni(NH_3)_6(OH)_2$ is transferred to a desiccator containing concentrated H_2SO_4 and kept there for several days. Slow removal of the NH_3 by H_2SO_4 yields well-formed glassy flakes of β-$Ni(OH)_2$ [21]. α-$Ni(OH)_2$ can be prepared electrochemically. This can be converted to β-$Ni(OH)_2$ by heating in 6-9M KOH at 90°C for 2-3 hours [11].

The definitive structural determination of the β-hydroxide is the powder neutron diffraction work of Greaves and Thomas on β-$Ni(OD)_2$ [22]. They did neutron diffraction studies on well crystallized deuterated $Ni(OD)_2$ that had been prepared by a hydrothermal method. They also investigated a high surface area $Ni(OH)_2$ that was prepared by precipitation on addition of KOH to a $NiSO_4$ solution. The X-ray and neutron diffraction results indicate that β-$Ni(OH)_2$ has a brucite C6-type structure that is isomorphous with the divalent hydroxides of Ca, Mg, Fe, Co and Cd. The structure is shown in Fig. 2. The crystal consists of stacked layer of nickel-oxygen octahedra. The nickels are all in the (0001) plane and are surrounded by six hydroxyl groups, each of which is alternatively above and below the (0001) plane. The fractional coordinates are for nickel, 0,0,0 and, for oxygen, 1/3, 2/3, z and 2/3, 1/3, z. Values for the crystallographic parameters are given in Table 1. These are for well crystallized β-$Ni(OD)_2$.

Because of anomalous scattering by H the results for the as-precipitated $Ni(OH)_2$ could not be refined. Nevertheless, cell constants and the OH bond distance could be determined. The results showed that the as-precipitated material was different from the well crystallized material. The unit cell dimensions were a_o=3.119 Å and c_o=4.686 Å. Also the O-H bond length was 1.08 Å a value similar to that previously reported by Szytula et al. in a neutron diffraction study of $Ni(OH)_2$ [23]. The O-H bond in both well crystallized and the as precipitated materials is

parallel to the c-axis. The difference between well crystallized and as-precipitated material is important since the well crystallized material is not electrochemically active. The differences between the materials are attributed to a defective structure that accrues from the large concentration of surface OH^- ion groups in the high surface area material [22]. These are associated with absorbed water. This is consistent with an absorption band in the infrared at 1630 cm^{-1}. This is not seen in the well crystallized material.

Infrared spectroscopy has also confirmed the octahedral coordination of nickel by hydroxyl groups [24, 25]. No evidence was found for hydrogen bonding. In battery materials, evidence was also found for a small amount of absorbed water [24, 26]. Even though these materials contain small amounts of water they are still classified as β-$Ni(OH)_2$ because of a (001) x-ray reflection corresponding to a d spacing of 4.65 Å. Thermogravimetric analysis indicate that the water is removed at higher temperatures [26-28]. Kober [24, 26] has proposed that this water is associated with nickel ions in the lattice and proposed a formula $[Ni(H_2O)_{0.326}](OH)_2$ for the chemically prepared battery material. A similar formula was proposed by Dennstedt and Loser [27]. However, this has been disputed [29]. The evidence is that well crystallized β-$Ni(OH)_2$ does not contain absorbed water [22, 29]. However, the high surface area material that is used in batteries does. This is consistent with the expansion in the c-axis of the crystal from 4.593 Å to 4.686 Å, the increase in the average O-H bond distance from 0.973 Å to 1.08 Å [22] and the presence of a broad absorption band in the infrared spectrum at 1630 cm^{-1} [22, 24, 26]. TGA results indicate that this water is removed in a single process over a temperature range of 50° to 150°C [30].

The Raman spectroscopic work of Jacovitz [31], Cornilsen [32, 33] and Audemer et al. [34] is the most direct spectroscopic evidence that the discharge product in battery electrodes, operating on the β/β cycle, is different from well crystallized β-$Ni(OH)_2$. The OH stretching modes and the lattice modes in the Raman spectra are different from those found for well crystallized $Ni(OH)_2$, prepared by recystallization from the ammonia complex, and are more similar to those found for the initial material prepared by Barnard et al. [21] by precipitation of the $Ni(OH)_2$ by adding 3M $Ni(NO_3)_2$ to hot 7 M KOH. In discharged electrodes a Raman band at 3605 cm^{-1} is observed. This has been ascribed to adsorbed water molecules on the surface of the $Ni(OH)_2$ [34]. There have been discrepant results in the Raman evidence for adsorbed water. However, some water cannot be ruled out since the OH modes are very poor Raman scatters. Infrared spectroscopy is much better at detecting water and Jackovitz has seen water stretching modes in both the non deuterated and deuterated material after discharge [31]. Audermer have also seen this band at 1630 cm^{-1}. Furthermore, they have confirmed that both the Raman band at 3605 cm^{-1} and the IR band at 1630 cm^{-1} decrease at temperatures above 100°C and completely vanish at 150°C. Neutron diffraction work on $Ni(OH)_2$. Raman and IR spectroscopy clearly show that the discharge product in battery electrodes is closely related, but is not identical, to well crystallized β-$Ni(OH)_2$. It probably has a defect structure which facilitates water adsorption and the electrochemical reactions.

3.1.2 α-$Ni(OH)_2$

α-$Ni(OH)_2$ which has a highly hydrated structure was first identified by Lotmar and Fectknecht [35]. α-$Ni(OH)_2$ is a major component of the active material in battery electrodes when cathodic impregnation of nickel battery plaques is done from an aqueous $Ni(NO_3)_2$ solutions at temperatures below 60°C [36]. α-Ni(OH) can be prepared chemically by precipitation from dilute solutions at room temperature. One method is to simply add an ammonia solution to a nickel nitrate solution [20]. Another method is to add 0.5 or 1 M KOH to 1 M $Ni(NO_3)_2$ [21]. In both cases the precipitate is filtered and washed. Methods for electrochemical preparation of films α-$Ni(OH)_2$ on nickel substrates have been described [37, 38]. The method consists of cathodically polarizing a cleaned nickel sheet in a quiescent 0.1 M $Ni(NO_3)_2$ solution at 8 mA/cm^2 . There is reduction of nitrate and a concomitant increase in pH at the electrode surface. This causes precipitation of an adherent coating of α-$Ni(OH)_2$ on the nickel. A 100 s of deposition will produce 0.5 mg/cm^2 of α-$Ni(OH)_2$.

Determination of the structure of α-$Ni(OH)_2$ has been difficult since sometimes it exhibits no diffraction pattern [39]. After washing with water a diffuse pattern develops. Hydrothermal treatment eventually leads to well crystallized β-$Ni(OH)_2$ [39, 40]. The evolution of the x-ray diffraction patterns is shown Fig. 3. Bode proposed a layered structure for α-$Ni(OH)_2$ similar to that for β-$Ni(OH)_2$ (11). His proposed structure was essentially identical to that shown for β-$Ni(OH)_2$ in Fig. 2, except that between the (0001) planes there are water molecules that result in an expansion of the c-axis spacing to about 8 Å. Bode proposed a unit cell $3Ni(OH)_2 \cdot 2H_2O$ and assigned definite positions to the intercalated water molecules in which 2/3 of the available nickel sites were occupied with water molecules [39]. The model gives unit cell dimensions of a_o=5.42 Å and c_o=8.05 Å. In addition to the increase in c-axis spacing, Bode reported a small contraction in the lattice parameters within the layer planes of α-$Ni(OH)_2$. Later work by Figlarz et al., using the x-ray diffraction line profiles, showed that α-$Ni(OH)_2$ was turbostratic and that it consisted of brucite like layers randomly oriented along the c-axis [41]. Subsequently McEwan [19] also used line profile analysis to arrive at the same conclusion. He also concluded that the intercalated water layer was not ordered. He also disputed the contraction in the basal plane that was proposed by Bode, and ascribed the diffraction peak shifts to disorder and particle size effects. Le Bihan and Figlarz use a combination of x-ray diffraction, electron microscopy and infrared spectroscopy to study as prepared α-$Ni(OH)_2$ and after repeated washing in water [42]. They confirmed that in the α-structure the $Ni(OH)_2$ planes are essentially identical to those shown for β-$Ni(OH)_2$ in Fig. 2. The layers are stacked with random orientation. The c-axis spacing is constant but the layers are randomly oriented. The layer, are separated by water molecules that are hydrogen bonded to the Ni-OH groups in the basal planes. In electron micrographs turbostratic nickel hydroxide appears as thin crumpled sheets. The crystallites have a mean size of 30 Å along [0011] which corresponds to a stacking of five layers. The basal plane dimensions are about 80 Å [42]. Because of the high degree of division, α-$Ni(OH)_2$ retains adsorbed surface water and a small amount (<3%) of nitrate ions [43]. Thermogravimetric analysis indicates that the adsorbed water is removed between 50° to 90°C whereas the intercalated water is removed between 90° and 180°C [30].

Pandya et al. have used EXAFS to study both cathodically deposited α-$Ni(OH)_2$ and chemically prepared β-$Ni(OH)_2$ [44]. Measurements were done at both 77 K and 297 K. The results for β-$Ni(OH)_2$ are in agreement with the neutron diffraction data [22]. In the case of α-$Ni(OH)_2$ they found a contraction in the first Ni-Ni bond distance in the basal plane. The value was 3.13 Å for β-$Ni(OH)_2$ and 3.08 Å for α-$Ni(OH)_2$. The fact that a similar significant contraction of 0.05 Å was seen at both 77 K and 297 K when using two reference compounds (NiO and β-$Ni(OH)_2$) led them to conclude that the contraction was a real effect and was not an artifact due to structural disorder. They speculate that the contraction may be due to hydrogen bonding of OH groups in the brucite planes with intercalated water molecules. These ex situ results on α-$Ni(OH)_2$ were compared with in situ results in 1 M KOH. In the ex situ experiments the α-$Ni(OH)_2$ was prepared electrochemically washed with water and dried in vacuum. In the in situ experiment the hydroxide film was simply rinsed, without drying, after preparation and immediately immersed in the in situ cell containing 1 M KOH. The coordination numbers for Ni-O for the in situ samples were consistently higher. The significance of this is not clear. It might suggest some water association with nickel as was postulated by Kober [24, 27].

Raman spectroscopy results indicate that the structure of α-$Ni(OH)_2$ is very dependent on how it is prepared [32, 33, 45]. These authors have obtained data on chemically prepared [32, 33], cathodically deposited [32, 33, 45] and electrochemically reduces γ-NiOOH [32, 33, 45]. There are differences in all the spectra both in the lattice modes and the O-H stretching modes. The shifts in the lattice modes for the reduced γ-NiOOH may be due to this material having an oxidation state higher than two. The changes in the O-H stretching modes may be due to changes in water content and hydrogen bonding.

Figlarz and his co-workers have suggested that the formula $Ni(OH)_2 \cdot nH_2O$ is not the correct one for α-$Ni(OH)_2$ [46, 47]. They studied α-$Ni(OH)_2$ materials made by precipitation of the hydroxide by the addition of NH_4OH to solutions of various nickel salts. In addition to $Ni(NO_3)_2$ and $NiCO_2$ they used nickel salts with carboxylic anions of various sizes. They found that the interlaminar distance in the α-$Ni(OH)_2$ depended on the nickel salt anion size. For instance when the nickel adipate was used the interlaminar distance was 13.2 Å. Infrared studies of α-$Ni(OH)_2$ precipitated from $Ni(NO_3)_2$ indicated that NO_3^- was incorporated into the hydroxide and was bonded to Ni. They suggested a model based on hydroxide vacancies and proposed a formula $Ni(OH)_{2-x}A_yB_z \cdot nH_2O$ where A and B are mono or divalent anions and $x=y+2z$. Chemical analysis of α-$Ni(OH)_2$ precipitated from $Ni(NO_3)_2$ indicate OH vacancies in the range of 20 to 30%.

α-$Ni(OH)_2$ is unstable in water and is slowly converted to β-$Ni(OH)_2$. Transmission electron micrographs of the reactants and products indicate that the reaction proceeds through the solution [42, 45]. In concentrated KOH the reaction is much more rapid and the product has a smaller particle size. For instance the α-$Ni(OH)_2$ in a electrochemically impregnated battery electrode is completely converted to β-$Ni(OH)_2$ 30 minutes after immersion in 4.5 M KOH [36].

Infrared studies of the reaction product in water indicates that the β-$Ni(OH)_2$ that is initially formed also contains anions and adsorbed water. As the particle size of the product increases the amount of anions and adsorbed water decreases [45].

Delmas and co-workers have proposed the existence of an intermediate phase between α and β-$Ni(OH)_2$ [48]. This phase consist of interleaved α and β material and can be formed on ageing of α-$Ni(OH)_2$. Recent Raman results confirm the existence of such a phase [49].

3.1.3 β-NiOOH

β-NiOOH has been identified as the primary oxidation product of electrodes containing β-$Ni(OH)_2$ [11, 50, 51]. Glemser describes a method for preparation of β-NiOOH [52, 53]. A solution of 100 g of $Ni(NO_3)_2 \cdot 6H_2O$ in 1.5 l H_2O was added dropwise to a solution of 55 g KOH and 12 ml Br_2 in 300 ml of H_2O, while keeping the temperature at 25 °C. The black precipitate was washed with CO_2 free water until both K^+ and NO_3^- were removed and then dried over H_2SO_4. Structural determinations of the higher oxides of nickel are complicated because of their amorphous nature [53]. However, it appears that β-$Ni(OH)_2$ is oxidized to the trivalent state without major modifications to the brucite structure. The unit cell dimensions change from a_o=3.126 Å and c_o=4.605 Å for β-$Ni(OH)_2$ to a_o=2.82 Å and c_o=4.85 Å for β-NiOOH. X-ray diffraction clearly indicates expansion along the c-axis. Asymmetry in the hk lines indicate the turbostratic nature of β-NiOOH. Even after correcting the a_o values for this, McEwan found that there was a real contraction in the basal plane [19]. Transmission EXAFS has been used to investigate the oxidation products of β-$Ni(OH)_2$ [54, 55]. In situ measurements were done on plastic bonded electrodes. In the charged state a two shell fit was necessary for the first Ni-O coordination shell. This suggests that the oxygen coordination in β-NiOOH is a distorted octahedral coordination with four oxygens at a distance of 1.88 Å and two oxygens at a distance of 2.07 Å. The distorted coordination is consistent with the edge features of the X-ray absorption spectra [55, 56]. The overall reaction for the electrochemical formation of β-NiOOH is usually given as

$$\beta\text{-}Ni(OH)_2 + \beta\text{-}NiOOH + H^+ + e.$$

During the reaction, protons are extracted from the brucite lattice. Infrared spectra [24, 25, 31] show that during charge the sharp hydroxyl band at 3644 cm^{-1} disappears. This absorption is replaced by a diffuse band at 3450 cm-1. The spectra indicate a hydrogen bonded structure for β-NiOOH with no free hydroxyl groups. β-NiOOH probably has some adsorbed and absorbed water. However, TGA data on charged materials is very limited [57, 58] and it is not always clear that the material is pure β-NiOOH. Unless electrochemical experiments are done very carefully there is always the possibility of the presence of γ-NiOOH [13].

3.1.4 γ-NiOOH

γ-NiOOH is the oxidation product of α-$Ni(OH)_2$. It is also produced on overcharge of β-$Ni(OH)_2$ particularly when the charge is carried out at high rates in high concentrations of alkali

[11, 59]. The use of the lighter alkalis (LiOH and NaOH) favor the formation of γ-NiOOH whereas the use of RbOH inhibits its formation [60]. The material was first prepared by Glemser and Einerhand [52] by fusing one part Na_2O_2 with three parts NaOH in a nickel crucible at 600'C. Hydrolysis of the product yields γ-NiOOH. They gave cell dimensions for a rhombohederal system with a=2.8 Å and c=20.65 Å. The material has a layer structure with a spacing of 7.2 Å between layers. γ-NiOOH always contains small quantities of alkali metal ions and water in between the layers, whereas β-NiOOH does not. The x-ray diffraction patterns have more and much sharper lines than those of either α-$Ni(OH)_2$ or β-NiOOH [19, 53].

γ-NiOOH prepared by the method of Glemser and Einerhand has the formula NiOOH-0.51 H_20. TGA analysis shows that this water is lost between 50° and 180°C [58].

3.1.5 Relevance of Model Compounds to Electrode Materials

The reaction scheme of Bode [11] was derived by comparison of the x-ray diffraction patterns of the active materials with those for the model compounds. The previous section discusses how the β-$Ni(OH)_2$ in battery electrodes differs from the model compound. In recent years the arsenal of *in situ* techniques for electrode characterization has greatly increased. Most of the results confirm the reaction scheme of Bode and essentially all the features of the proposed α/γ cycle. For instance, recent atomic force microscopy (AFM) results on α-$Ni(OH)_2$ show results consistent with a contraction of the interlayer distance from 8.05 Å to 7.2 Å on charge [61-63]. These are the respective interlayer dimensions for the model α-$Ni(OH)_2$ and γ-NiOOH compounds. Also electrochemical quartz crystal microbalance (ECQM) measurements confirm the ingress of alkali metal cations into the lattice on the conversion of α-$Ni(OH)_2$ to γ-NiOOH [45, 64, 65]. However, in situ Raman and surface enhanced Raman (SERS) results on electrochemically prepared α-$Ni(OH)_2$ in 1 M NaOH show changes in the OH stretching modes that are consistent with a weakening of the OH bond when compared with results for the model α- and β-$Ni(OH)_2$ compounds [66]. This has been ascribed to the delocalization of protons by intercalated water and Na^+ ions. Similar effects have been seen in passive films on nickel in borate buffer electrolytes [67].

Recent ECQM work and x-ray diffraction have confirmed the conversion of the α/γ cycle to the β/β cycle on electrochemical cycling in concentrated alkali. Earlier ECQM studies of α-$Ni(OH)_2$ films had shown a mass inversion in the microgravimetric curve after prolonged cycling [64]. After prolonged cycling there is a mass decrease on charge instead of a mass increase. More recent work has confirmed that the mass inversion is due to conversion of the α/γ cycle to the β/β cycle [65].

3.2 Pyroaurite Type Nickel Hydroxides.

Allmann found that when suitable trivalent ions were introduced during the precipitation of the hydroxides of Mg, Zn, Mn, Fe, Co and Ni, these were incorporated in the lattice and the structure changed from the brucite ($Mg(OH)_3$) to the pyroaurite ($[Mg_6Fe_2(OH)_{16}]\cdot[CO_3\cdot\sim 4H_2O]$) type structure [68]. One of the nickel materials he prepared was a Ni/Al hydroxide. Axmann et al. [69-71] have given the nickel compounds the general formula

$$[Ni_{1-x}^{II}M_x^{III}(OH)_2]^{x+}[(X^{n-})_{x/n}(H_2O)_z]^{x-}$$
$$K^{x+} \qquad A^{x-}$$

where $0.2 \leq x \leq 0.4$ and X are the anions of the precursor salts. The resultant structure consists of brucite cationic layers intercalated with anions and water molecules. The cationic nature of the brucite layers are due to the higher valence of the substituent cations and the anions in the intercalated anion layers provide electroneutrality. As a result the interlayer distance increases from 4.68 Å to 7.80 Å when compared to β-$Ni(OH)_2$. The structure is shown schematically in Fig. 4. Electrochemical and chemical oxidation transforms the pyroaurite structure to a product that is isostructural with γ-NiOOH [72].

In the early work the pyroaurite compounds were prepared by precipitation. Buss et al. report on the preparation of $Ni_4Al(OH)_{10}NO_3$ prepared in a computer controlled apparatus wherein a solution of 0.4 m $Ni(NO_3)_2 \cdot 6H_2O$ + 1 M $Al(NO_3)_3 \cdot 9H_2O$ in doubly distilled water with the pH adjusted to pH 2 with 1 M HNO_3 was simultaneously sprayed with a carbonate free 1 M KOH solution into a receptor solution whose pH was maintained at pH 11.5 and a temperature of 32°C [70, 71]. The precipitate was filtered, washed and dried at 50°C for 3 days at 0.01 bar and carbon dioxide was excluded at all stages of the preparation.

Delmas and his co-workers have done extensive work on pyroaurite type materials. The work has recently been reviewed [73]. In addition to precipitation methods they have prepared the materials by mild oxidative hydrolysis of nickelates that were prepared by thermal methods similar to those used for the preparation of $LiNiO_2$ [74]. A cobalt substituted material ($NaCo_xNi_{1-x}O_2$) was prepared by the reaction of Na_2O. Co_3O_4 and NiO at 800°C under a stream of oxygen. The material was then treated with a 10 M NaClO + 4 M KOH solution for 15 h to form the oxidized γ-oxyhydroxide. The pyroaurite phase was prepared by subsequent reduction in a solution of 0.1 M H_2O_2 in 4 M KOH [75]. These mild chemical treatments are referred to as "chemie douche" reactions [69]. The thermally prepared nickelates have a layered R3m structure. The "chemie douche" treatments essentially leave the covalently bonded $Co_xNi_{1-x}O_2$ layers intact. As a result more crystalline materials with larger particle sizes can be made with this method.

Most of the work on pyroaurite materials has been done on materials with Fe [68-72, 76, 77], Co [68, 75, 78], Mn [72, 79] or Al [68, 70, 72] substitutions. When at least 20% on the Ni atoms are replaced by the trivalent substituent the materials are stable in concentrated KOH. In many ways the pyroaurite phase is similar to α-$Ni(OH)_2$. Thus substitution of 20% if the Ni with these trivalent ions stabilizes the operation of the electrode in the α/γ cycle in concentrated KOH.

Because of the possibility of doing Mössbauer spectroscopy the solid state chemistry of the Fe substituted material is best understood [69, 72, 77]. Mössbauer spectroscopy confirms that the Fe in the pyroaurite type material is Fe(III). Glemser and coworkers have found that electrochemical or electrochemical oxidation of the material converts about 30% of the Fe(III) to

Fe(IV) [69, 72]. The results were consistent with a high-spin configuration with the Fe(IV) in FeO_6 octahedra with O_h symmetry. The O_h symmetry can only occur if the surrounding NiO_6 octahedra also have an O_h symmetry. Hence the Fe(IV) ions in the layer must be surrounded by six NiO_6 octahedra with the Ni in the Ni(IV) state. Delmas and coworkers found evidence for Fe(IV) in both high- and low-spin states for oxidized materials prepared by the "chemie douche" method [77]. The different results may be due to the effect of the platelet size in the pyroaurite structure.

In the pyroaurite structure the brucite layers are cationic. However, on oxidation the resultant brucite layers in γ-NiOOH are anionic. To preserve electroneutrality, cations and anions are exchanged in the intercalated layer during the oxidation-reduction process. This is illustrated in Fig. 4. In the case of Mn substituted materials, the Mn some Mn can be reduced to Mn(II). This neutralizes the charge in the brucite layer and this part of the structure reverts to the β-$Ni(OH)_2$ structure and the intercalated water and anions are expelled from the lattice. With this there is a concomitant irreversible contraction of the interlayer spacing from 7.80 Å to 4.65 Å [72].

4. Electrochemical Reactions

4.1 Overall Reaction and Thermodynamics of the $Ni(OH)_2$/NiOOH Couple

In normal battery operation several electrochemical reactions occur on the nickel hydroxide electrode. These are the redox reactions of the active material, oxygen evolution, and in the case of nickel-hydrogen and metal hydride batteries hydrogen oxidation. In addition there are parasitic reactions such as the corrosion of nickel current collector materials and the oxidation of organic materials from separators. The initial reaction in the corrosion process is the conversion of Ni to $Ni(OH)_2$.

Because of the complexity of the redox reactions they cannot be conveniently presented in a Pourbaix pH-potential diagram. For battery applications the revised diagram given by Silverman [80] is more correct than that found in the Pourbaix Atlas [81]. The diagram is shown in Fig. 5. The respective literature values for the free energy of formation of $Ni(OH)_2$, NiOOH, H_2O and HgO are -78.71, -109.58, -56.69 and -13.98 kcal/mole [80]. The calculated $Ni(OH)_2$/NiOOH reversible potential is 0.41 V vs. Hg/HgO. The reversible oxygen potential is 0.30 V vs. Hg/HgO. Unlike other battery positive electrode materials, such as AgO or PbO, the nickel hydroxide electrode is a good catalyst for oxygen evolution. Towards the end of charge oxygen evolution occurs in all nickel batteries, and during charge stand self discharge occurs via a couple involving the reduction of NiOOH and the oxidation of water to oxygen.

The self discharge process has made experimental determination of the reversible potential of the $Ni(OH)_2$/NiOOH couple very difficult. A major advance was the realization by Bourgault and Conway that the open circuit potential of a charged nickel oxide electrode was a mixed potential not a true equilibrium potential [82]. This potential is the result of two processes which are the discharge of NiOOH and oxygen evolution. They devised an extrapolation technique for

the determination of the open circuit potential of Ni(OH)2 as a function of charge state. Later the work was expanded by Barnard and his co-workers to include oxidation of both α/γ and the β/β couples [83]. The open circuit potentials depended on pretreatments such as formation cycles and ageing in concentrated KOH electrolytes. The β/β couples had open circuit potentials in the range of 0.44 to 0.47 V vs. Hg/HgO whereas the α/γ couples had values in the range of 0.39 to 0.44 V. In cyclic voltammetry experiments the respective anodic and cathodic peaks for the α/γ couple occur at 0.43 V and 0.34 V. For the β/β couple the peaks are at 0.50 V and 0.37 V. The reversible potentials of the β/β couple are essentially invariant with KOH concentration whereas those of the α/γ couple vary with OH^- concentration and aging of α-$Ni(OH)_2$ reduces the OH^- dependence of the reversible potential [84] This is due to the conversion to the β/β couple.

The reactions for both the β/β and the α/γ couples are highly reversible. Barnard and Randell, in a simple experiment, showed that β-NiOOH could oxidize α-$Ni(OH)_2$ to γ-NiOOH [85]. This reaction is possible while doing cyclic voltammetry on α-$Ni(OH)_2$ thin film electrodes in KOH electrolyte, and some of the α material gets transformed to the β form. This could account for the negative drift that is seen in the anodic peaks in the early stages of cycling [66]. Reactions of this type can introduce distortions and features in cyclic volammograms that are difficult to interpret.

4.2 Nature of the $Ni(OH)_2$/NiOOH Reaction

The $Ni(OH)_2$/NiOOH reaction is a topochemical type of reaction that does not involve soluble intermediates. Many aspects of the reaction are controlled by the electrochemical conductivity of the reactants and products. Photoelectrochemical measurements [86,87] indicate that the discharged material is a p-type semiconductor with a band gap of about 3.7 eV. The charged material is an n-type semiconductor with a bandgap of about 1.75 eV. The bandgaps are estimates from absorption spectra [87]. The simple experiments of Kuchinskii and Ershler have provided great insights into the nature of the Ni(OH)2/NiOOH reaction [88, 89]. They investigated oxidation and reduction of a single grain of $Ni(OH)_2$ with a platinum point contact. On charge, the $Ni(OH)_2$ turned black and oxygen was evolved preferentially on the black material and not on the platinum. This implies that NiOOH is conductive and has a lower oxygen overvoltage than platinum oxide. On discharge, they found that discharge started at the point contact and that formation of resistive $Ni(OH)_2$ at this interface could stop current flow and result in an incomplete discharge. These results provide a good macroscopic picture of how the electrode works. This type of mechanism has been considered by Barnard *et al* [83]. They postulate the initiation of the charging reaction at the $Ni(OH)_2$/current collector interface with the formation of a solid solution of Ni^{+3} ions in $Ni(OH)_2$. With further charging when a fixed nickel ion composition $Ni^{2+}_x \bullet Ni^{3+}_{(1-x)}$ is reached phase separation occurs with the formation two phases, one with the composition $Ni^{2+}_{(1-x)} \bullet Ni^{3+}_{(x)}$ in contact with the current collector, the other with the composition $Ni^{2+}_x \bullet Ni^{3+}_{(1-x)}$ further out into the active mass. This scheme is consistent with the observations of Briggs and Fleischman on thick α-$Ni(OH)_2$ films [90]. In microscopic observations of cross-sections of partially charged electrodes, they observed a green layer of uncharged $Ni(OH)_2$ in front of the electrode. The central part of the electrode had a black

colored material and a thin layer in contact with the current collector had a yellowish metallic luster. On discharge the reverse process occurs. it is possible for some of the NiOOH to be isolated in the poorly conducting matrix of $Ni(OH)_2$ and not be discharge. This has been confirmed in recent in situ Raman spectroscopy studies [66].

Sometimes two discharge voltage plateaus are seen on nickel oxide electrodes. Early observations are documented in previous reviews [2, 9]. Normally nickel oxide electrodes have a voltage plateau on discharge in the potential ranges of 0.25 V to 0.35 V vs Hg/HgO. The second plateau. which in some cases can account for up to 50% of the capacity occurs at -0.1 V to -0.6 V. At present there is a general consensus that this second plateau is not due to the presence of a new less active compound [91-94]. Five interfaces have been identified for a discharging NiOOH electrode [93]. These are (a) the Schottky junction between the current collector and the n-type NiOOH, polarized in the forward direction, (b) the p-n junction between $Ni(OH)_2$ and NiOOH, polarized in the forward direction, (c) the NiOOH/electrolyte interface, (d) the $Ni(OH)_2$/electrolyte interface and (e) the Schottky junction between the current collector and $Ni(OH)_2$, polarized in the forward direction. At the beginning of discharge only junctions (a) and (c) are present. As discharge progresses junction (e) develops. The passage of current shifts the electrode potential to more negative values. The hole conductivity of the $Ni(OH)_2$ increases and a second discharge plateau appears. A quantitative modeling effort by Zimmerman [94] supports this hypothesis.

4.2 Nickel Oxidation State

Like all other facets of the electrode determination of the overall redox process has been difficult and many aspects are still disputed. The presence of Ni(IV) species in charged materials has been proposed by many authors. The early work has been reviewed [9]. The evidence for Ni(IV) is based mostly on coulometric data [95] or determinations of active oxygen by titration with iodide or arsenious oxide. Active oxygen contents corresponding to a nickel valence of 3.67 have been reported for α-$Ni(OH)_2$ films charged in 1 M KOH [95] and values of 3.48 were found for overcharged β-$Ni(OH)_2$ battery electrodes in 11 M KOH [96]. When these electrodes of high active oxygen content are discharged or even overdischarged an appreciable amount of active oxygen remains (57). Cycling between a nickel valence of 2.5 and 3.5 has been proposed (97). X-ray absorption has been used to study the problem [98,99]. In one case results consistent with a Ni oxidation state of 3.5 were found for a charged electrode [99]. In the case of the α/γ couple indications are that a nickel oxidation state of at least 3.5 can be reached on charge. It is not clear that this is the case with the β/β couple. In situ experiments with simultaneous x-ray diffraction and x-ray absorption measurements should be done on the β/β couple to check for the presence of γ-NiOOH. Also experiments on materials stabilized with both Co and Zn additives are necessary.

The existence of these high nickel oxidation state offers the possibility of a "two electron" electrode. This is one of the incentives for stabilizing the α/γ cycle through the use of the pyroaurite structures [73]. Using this approach it has been possible to achieve a 1.2 electron exchange for the overall reaction. However none of the pyroaurite structures are satisfactory for

battery electrodes. The Co and Mn substituted materials are unstable with cycling [72, 73]. The end of charge voltages for both the Fe and Al substituted materials are high and the charging efficiencies are low [72, 73]. However, the use of mixed substitution, such as combinations of Co and Al, can lower the charging voltage [73].

4.2 Oxygen Evolution

Oxygen evolution occurs on nickel oxide electrodes throughout charge, on overcharge and on standby. It is the anodic process in the self discharge reaction of the positive electrode in nickel cadmium cells. Early work in the field has been reviewed [9]. No significant new work has been reported in recent years.

4.4 Hydrogen Oxidation

The reaction of hydrogen at the nickel electrode determines the rate of self discharge in nickel-hydrogen batteries. Under the typical operating pressures (30-50 Atm.) a nickel hydrogen battery will loose 50% of its capacity in a week. The self discharge is about five times that encountered in sealed nickel-cadmium batteries, where the rate determining step is oxygen evolution [100]. Tsenter and Sluzhevskii [101] developed a set of kinetic equations to describe the self discharge process. in their model the self discharge rate depends on the hydrogen pressure and the amount of undischarged NiOOH in the cell. Experimental results of Srinivasan and co-workers confirm many aspects of this model [102]. They used a combination of microcalorimetry, open circuit voltage measurements and capacity measurements to study the problem. By doing measurements on the active material and substrate, separately and combined. they were able to establish that hydrogen oxidation occurs predominantly on the charged active material with simultaneous reduction of the oxide.

Acknowledgment

This research was performed under the auspices of the U.S. Department of Energy, Division of Materials Sciences, Office of Basic Energy Sciences under Contract No. DE-AC02-76CH00016.

References

1. S.U. Falk and A.J. Salkind, *Alkaline Storage Batteries*, Wiley, New York, 1969.

2. P.C. Milner and U.B. Thomas, in *Advances in Electrochemistry and Electrochemical Engineering* [Ed.: C.W. Tobias], Wiley, New York, 1967, p. 1.

3. G.W.D. Briggs, *in Electrochemistry - Vol. 4, Specialist Periodical Reports*, The Chemical Society, London, 1974, p. 33.

4. A.J. Arvia and D. Posadas, in *Encyclopedia of Electrochemistry of the Elements, Vol. III* [Ed.: A.J. Bard], Marcel Dekker, New York, 1975, p. 212.

5. J.L. Weininger, in *Proceedings of the Symposium on the Nickel Electrode* [Eds.: R.G. Gunther and S. Gross], The Electrochemical Society, Pennington, N.J., 1982, p. 1.

6. P. Oliva, J. Leonardi, J.F. Laurent, C. Delmas, J.J. Bracconier, M. Figlarz, F. Fievet and A. de Guibert, *J. Power Sources* **1982**, 8, 229.

7. G. Halpert, *J. Power Sources* **1984**, 12, 177.

8. G. Halpert, *Proceedings of the Symposium on Nickel Hydroxide Electrodes* [Eds.: D. A. Corrigan and A. H. Zimmerman], The Electrochemical Society, Inc. Pennington, NJ, **1990**, pp. 3-17.

9. J. McBreen, in *Modern Aspects of Electrochemistry*, Vol. 21 [Eds.: R.E. White, J. O'M. Bockris and B.E. Conway], Plenum Press, New York, **1990**, pp. 29-64.

10. A. H. Zimmerman, *Proceedings of Symposium on Hydrogen and Metal Hydride Batteries* [Eds.: P. D. Bennett and T. Sakai], The Electrochemical Society, Inc. Pennington, NJ, **1994**, pp. 268-283.

11. H. Bode, K. Dehmelt and J. Witte, *Electrochim. Acta* **1966**, 11, 1079.

12. A. H. Zimmerman and A. H. Phan, *Proceedings of Symposium on Hydrogen and Metal Hydride Batteries* [Eds.: P. D. Bennett and T. Sakai], The Electrochemical society, Inc. Pennington, NJ, **1994**, pp. 341-352.

13. M. Oshitani, H. Yufu, K. Takashima, S. Tsuji and Y. Matsumaru, *J. Electrochem. Soc.* **1989**, 136, 1590

14. W. A. Ferrando. *J. Electrochem. Soc.* **1985**, 132, 2417

15. H. Watada, M. Ohnishi, Y. Harada and M. Oshitani, *Proceedings of the 25th IECEC Meeting*, IEEE, Piscataway, NJ, **1990**, pp. 299-304.

16. M. Oshitani and H. Yufu, U.S. Patent 4844999, **1989**.

17. A. Fleischer, *Trans. Electrochem. Soc.* **1948**, 94, 289.

18. M. Aia, *J. Electrochem. Soc.* **1966**, 113, 1045.

19. R.S. McEwen, *J. Phys. Chem.* **1971**, 75, 1782.

20. F. Fievet and M. Figlarz, *J. Catal.* **1975**, 39, 350.

21. R. Barnard, C.F. Randell and F.L. Tye, in *Power Sources 8* [Ed.: J. Thompson], Academic Press. London, **1981**, p. 401.

22. C. Greaves and M.A. Thomas, *Acta Cryst.* **1986**, B42, 51.

23. A. Szytula, A. Murasik and M. Balanda, *Phys. Stat. Sol.* **1971**, 43, 125.

24. F.P. Kober, *J. Electrochem. Soc.* **1965**, 112, 1064.

25. F.P. Kober, *J. Electrochem. Soc.* **1967**, 114, 215.

26. F.P. Kober, in *Power Sources 1966* [Ed.: D.H. Collins], Pergammon Press, Oxford, **1967**, p. 257.

27. W. Dennstedt and W. Loser, *Electrochim. Acta*, **1971**, 16, 429.

28. B. Mani and J.P. de Neufville, *Mat. Res. Bull.* **1984**, 19, 377.

29. S. Le Bihan and M. Figlarz, *Electrochim Acta*, **1973**, 18, 123.

30. B. Mani and J.P. deNeufville, *J. Electrochem. Soc.* **1988**, 135, 801.

31. J.F. Jackovitz, in *Proceedings of the Symposium on The Nickel Electrode* [Eds.: R.G. Gunther and S. Gross], The Electrochemical Society, Inc., Pennington, NJ, **1982**, p. 48.

32. B.C. Cornilsen, P.J. Karjala, and P.L. Loyselle, *J. Power Sources* **1988**, 22, 351.

33. B.C. Cornilsen, X.-Y. Shan, and P.L. Loyselle, J. *Power Sources* **1990**, 29, 453.

34 H. Audemer, A. Delahaye, R. Farhi, N. Sac-Epée and J-M. Tarascon, *J. Electrochem. Soc.*, **1997**, 144, 2614.

35. Lotmar and W. Fectknecht,. *Kristallogr. Mineral. Petroga. Abt. Z* **1936**, A93, 368.

36. F. Portemer, A. Delahaye-Vidal and M. Figlarz, *J. Electrochem. Soc.* **1992**, 139, 671.

37. D. M. MacArthur, *J. Electrochem. Soc.* **1970**, 117, 422.

38. D.A. Corrigan, *J. Electrochem. Soc.* **1987**, 134, 377.

39. H. Bode, *Angew. Chem.* **1961**, 73, 553.

40. S. Le Bihan, J. Guenot and M. Fialarz, *C.R. Acad. Sci.* **1970**, C270, 2131.

41. M. Figlarz and S. Le Bihan, *C.R. Acad. Sci.* **1971**, C272, 580.

42. S. Le Bihan, and M. Figlarz, *J. Cryst. Growth*, **1972**, 13/14, 458.

43. A Delahaye-Vidal and M. Figlarz, *J. Appl. Electrochem.* **1987**, 17, 589.

44. K.I. Pandya, W.E. O'Grady, D.A. Corrigan, J. McBreen and R.W. Hoffman, *J. Phys. Chem.* **1990**, 94, 21.

45. S. I. Cordoba-Torresi, C. Gabrielli, A. Hugot-Le Goff and R. Torresi, *J. Electrochem. Soc.* **1991**, 138, 1548.

46. P. Genin, A Delahaye-Vidal, F. Portemer, K. Tekkia-Elhsissen and M. Figlarz, *Eur. J. Solid State Inorg. Chem.* **1991**, 28, 505

47. A Delahaye-Vidal, B. Beaudoin, N. Sac-Epée, K. Tekkia-Elhsissen, A. Audemer and M. Figlarz, *Solid State Ionics*, **1996**, 84, 239.

48. C. Faure, C. Delmas and M. Fouassier, *J. Power Sources*, **1991**, 35, 279.

49. M. C. Bernard, P. Bernard, M. Keddam, S. Senyarich and H. Takenouti, *Electrochim. Acta*, **1996**, 41, 91.

50. G.W.D. Briggs and W.F.K. Wynne-Jones, *Trans. Faraday Soc.* **1956**, 52, 1273.

51. S.U. Falk, *J. Electrochem. Soc.* **1960**, 107, 661.

52. O. Glemser and J. Einerhand, *Z. Anorg. Chem.* 261 (1950) 26.

53. C.A. Melandres, W. Paden, B. Tani and W. Walczak, *J. Electrochem. Soc.* 134 (1987) 762.

54. J. McBreen, W.E. O'Grady, K.I. Pandya, R.W. Hoffman and D.E. Sayers, *Langmuir* **1987**, 3, 428.

55. K.I. Pandya, R.W. Hoffman, J. McBreen and W.E. O'Grady, *J. Electrochem. Soc.*, **1990**, 137, 383.

56. J. McBreen, W.E. O'Grady, G. Tourillon, E. Dartyge, A. Fontaine and K.I. Pandya, *J. Phys. Chem.* **1989**, 93, 6308.

57. M. Aia, *J. Electrochem. Soc.* **1965**, 112, 418.

58. C. Greaves, M.A. Thomas and M. Turner, *Power Sources 9* [Ed.: J. Thompson], Academic Press, London, **1983**, p. 163.

59. J.P. Harivel, B. Morignat, J. Labat and J.F. Laurent, in *Power Sources 1966*, Ed.: D.H. Collins], Pergamon Press, Oxford, **1967**, p. 239.

60. H. S. Lim, S. A. Verzwyvelt and S. K. Clement, *Proceedings of the 23rd IECEC Meeting, Vol. 2*, American Society of Mechanical Engineers, New York, **1988**, pp. 457-463.

61. R.-R. Chen, Y. Mo and D.A. Scherson, *Langmuir*, **1994**, 10, 3933.

62. P. Häring and R. Kötz, *J. Electroanal. Chem.* **1995**, 385, 273.

63. A. Kowal, R. Niewiara, B. Peronczyk and J. Haber, *Langmuir*, **1996**, 12, 2332.

64. Y. Mo, E. Hwang and D. A. Scherson, *J. Electrochem. Soc.* **1996**, 143, 37.

65. M. S. Kim, T. S. Hwang and K B. Kim, *J. Electrochem. Soc.* **1977**, 144, 1537.

66. R. Kostecki and F. McLarnon, *J. Electrochem. Soc.* **1997**, 144, 485.

67. L. J. Oblonsky and T. M. Devine, *J. Electrochem. Soc.* **1995**, 142, 3677.

68. R. Allmann, *Chimia*, **1970**, 24, 99.

69. P. Axmann, C. F. Erdbrügger, D. H. Buss and O. Glemser, *Angew. Chem. Int. Ed. Engl.* **1996**, 35, 1115.

70. D. H. Buss, W. Diembeck and O. Glemser, *J. Chem. Soc., Chem. Commun.* **1985**, 81.

71. O. Glemser, D. H. Buss and J. Bauer, US Patent 4735629, **1988**.

72. P. Axmann and O. Glemser, *J. Alloys and Compounds*, **1997**, 246, 232.

73. C. Delmas, C. Faure, L. Gautier, L. Guerlou-Demourgues and A. Rougier, *Phil. Trans. R. Soc. Lond.* **1996**, 354A, 1545.

74. T. Ohzuku, A. Ueda and Nagayama, *J. Electrochem. Soc.* **1993**, 140, 1862.

75. C. Delmas, J. J. Braconnier, Y. Borthomeiu and P. Hagenmuller, *Mat. Res. Bull.* **1982**, 17, 117.

76. L. Demourges-Guerlou and C. Delmas, *J. Electrochem. Soc.* **1994**, 141, 713.

77. L. Demourges-Guerlou, L. Fournès and C. Delmas, *J. Solid State Chem.* **1995**, 114, 6.

78. C. Delmas, C. Faure and Y. Borthomeiu, *Mat. Sci. Eng.*, **1992**, B13, 89

79. L. Guerlou-Demourgues and C. Delmas, *J. Electrochem. Soc.*1996, 143, 561.

80. D.C. Silverman, *Corrosion* **1981**, 37, 546.

81. E. Deltombe, N. de Zoubov and M. Pourbaix, in *Atlas of Electrochemical Equilibria in Aqueous Solutions* [Ed.: M. Pourbaix], NACE, Houston, TX, **1974**, p. 330

82. P.L. Bourgault and B.E. Conway, *Can. J. Chem.* **1960**, 38, 1557.

83. R. Barnard, C.F. Randell and F.L. Tye, *J. Appl. Electrochem.* **1980**, 10, 109.

84. R. Barnard, C.F. Randell and F.L. Tye, *J. Electroanal Chem.* **1981**, 119, 17.

85. R. Barnard and C.F. Randell, *J. Appl. Electrochem.* **1983**, 13, 97.

86. M.J. Madou and M.C.H. McKubre, *J. Electrochem. Soc.* **1983**, 130, 1056

87. M.K. Carpenter and D.A. Corrigan, *Abstract No. 490 of papers presented at the Atlanta Meeting of the Electrochem. Soc.*, May 15-20, **1988**, p. 700.

88. E.M. Kuchinskii and B.V. Erschler, *J. Phys. Chem. (U.S.S.R.)*, **1940**, 14, 985.

89. E.M. Kuchinskii and B.V. Erschler, *Zhur. Fiz. Khim.* **1946**), 20, 539.

90. G.W.D. Briggs and M. Fleischman, *Trans. Faraday Soc.* **1971**, 67, 2397.

91. B. Klapste, J. Mrha, K. Micka, J. Jindra and V. Maracek, *J. Power Sources*, **1979**, 4, 349.

92. R. Barnard, G.T. Crickmore, J.A. Lee and F.L. Tye, *J. Appl. Electrochem.* **1980**, 10, 61.

93. B. Klapste, K. Micka, J. Mrha and J. Vondrak, *J. Power Sources*, **1982**, 8, 351.

94. A. H. Zimmerman, *Proc. 29th IECEC Meeting*, American Institute of Aeronautics and Astronautics, Inc. **1994**, pp. 63-68.

95. J. Desilvestro, D.A. Corrigan and M.G. Weaver, *J. Electrochem. Soc.* **1988**, 135, 885.

96. D. Tuomi, *J. Electrochem. Soc.* **1965**, 112, 1.

97. D. A. Corrigan and S. L. Knight, *J. Electrochem. Soc.* **1989**, 136, 613.

98. A. N. Mansour, C. A. Melandres, M. Pankuch and R. A. Brizzolara, *J. Electrochem. Soc.* **1994**, 141, L69.

99. W. E. O'Grady, K. I. Pandya, K. E. Swider and D. A. Corrigan, *J. Electrochem. Soc.* **1996**, 143, 1613.

100. S. Font and J. Goulard, in *Power Sources 5*, [Ed.: D.H. Collins], Academic Press, London, **1975**, p. 331.

101. B.I. Tsenter and A.I. Sluzhevskii, *Elektrokhimiya*, **1980**, 54, 2545.

102. Y. J. Kim, A. Visintin, S. Srinivasan and A. J. Appleby, *J. Electrochem. Soc.* **1992**, 139, 351.

Table I
Crystallographic Parameters for β-$Ni(OD)_2$ (22).

Parameter	Value
a_o(Å)	3.126
c_o(Å)	4.593
Ni-O bond length (Å)	2.073
O-H bond length (Å)	0.973
Ni-Ni bond length (Å)	3.126

Figure Captions

1. Reaction scheme of Bode (11).

2. The brucite structure of $Ni(OH)_2$. (a) The hexagonal brucite layer, small circles are the Ni atoms and the large circles the O atoms. Alternate O atoms are below and above the plane of the Ni atoms. (b) The stacking of the planes showing the orientation of the O-H bonds.

3. X-ray diffraction patterns (Co K_α) for (a) as precipitated α-$Ni(OH)_2$ and (b), to (d) the increase on crystallinity with time when aged in water. The pattern (e) for β-$NiOH)_2$ eventually develops (42).

4. Structure of the Fe(III) substituted pyroaurite phase in the discharged (α) and charged (γ) state. The edge shared NiO_6 and FeO_6 octahedra are shown. Also shown are the incorporation of anions and water in the galleries of the discharged material. On charge the anions are replaced by cations (77).

5 The modified Pourbaix diagram for Ni (80).

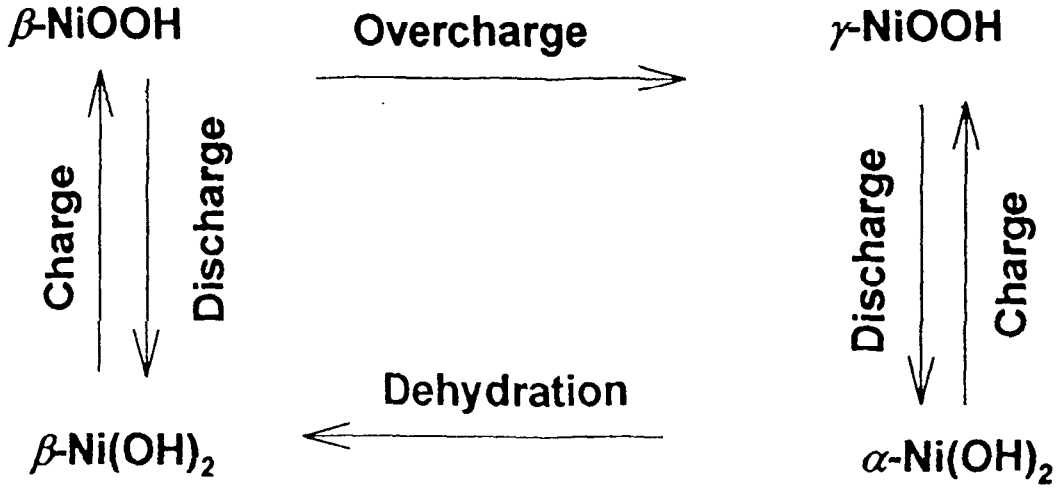
β-NiOOH
Overcharge
γ-NiOOH
Charge
Discharge
Discharge
Charge
Dehydration
β-Ni(OH)2
α-Ni(OH)2

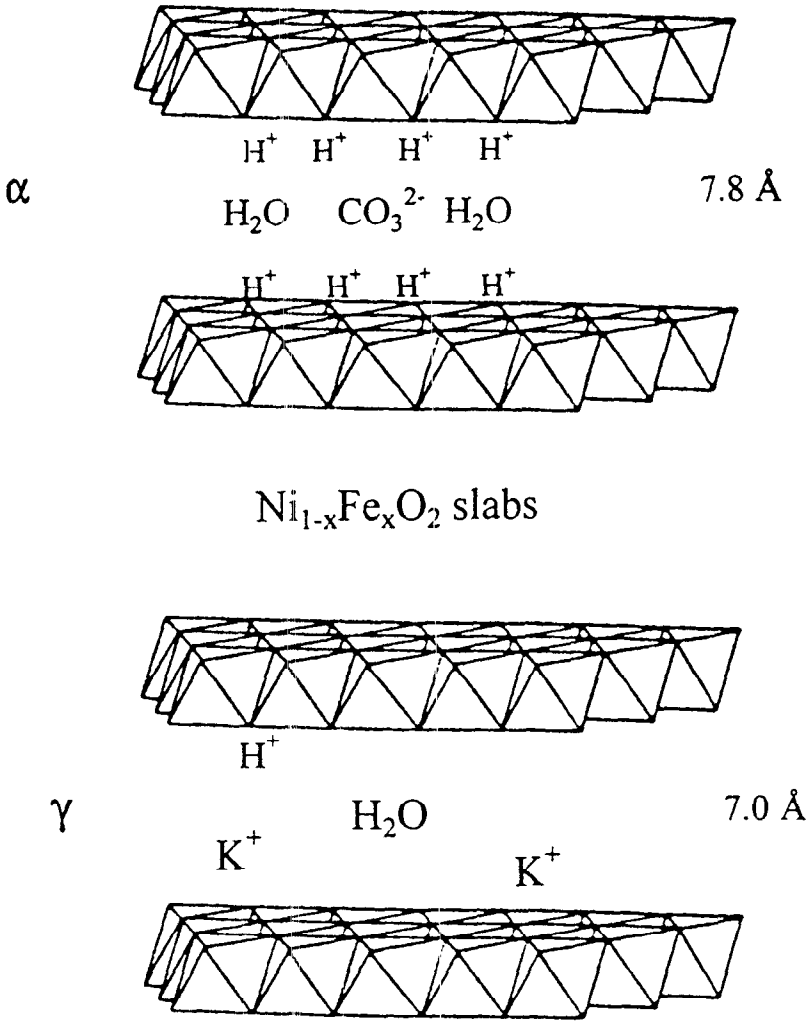
H+ H+ H+ H+
α
H2O CO3 2- H2O
7.8 Å
H+ H+ H+ H+
Ni1-xFexO2 slabs
H+
γ
H2O
7.0 Å
K+
K+

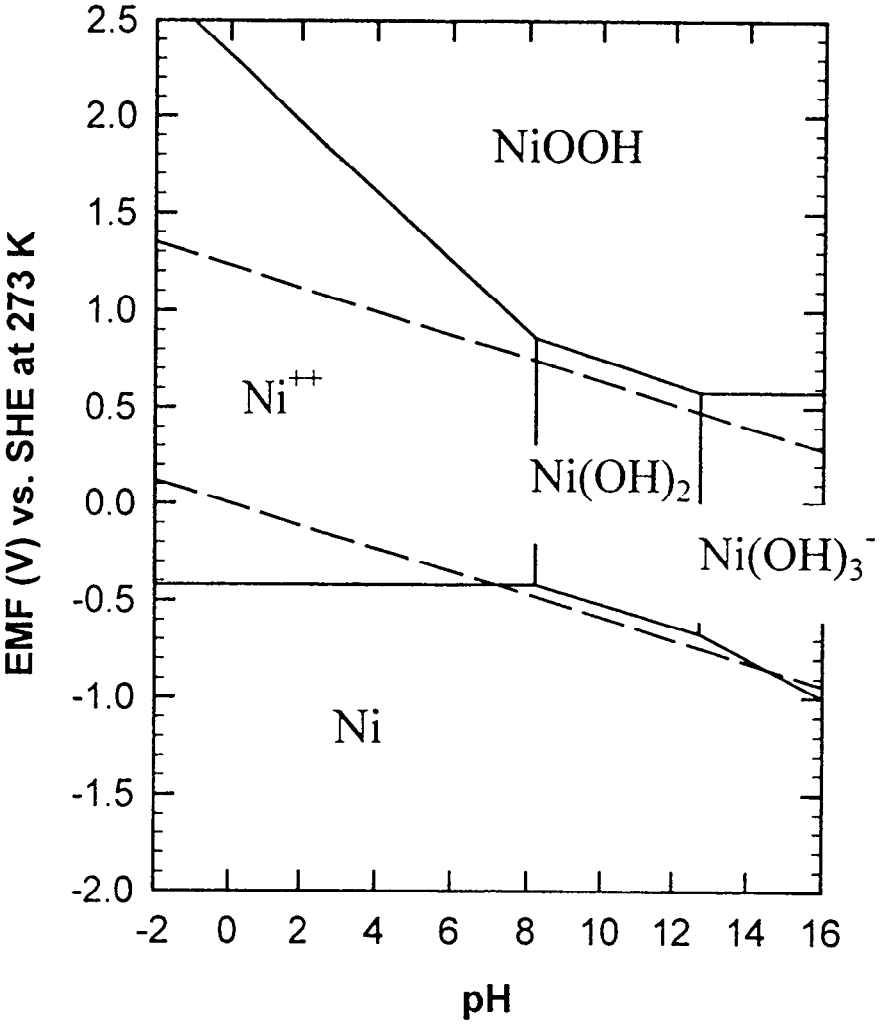
EMF (V) vs. SHE at 273 K
2.5
2.0
1.5
1.0
0.5
0.0
-0.5
-1.0
-1.5
-2.0
-2
0
2
4
6
8
10
12
14
16
pH
NiOOH
Ni++
Ni(OH)2
Ni(OH)3-
Ni

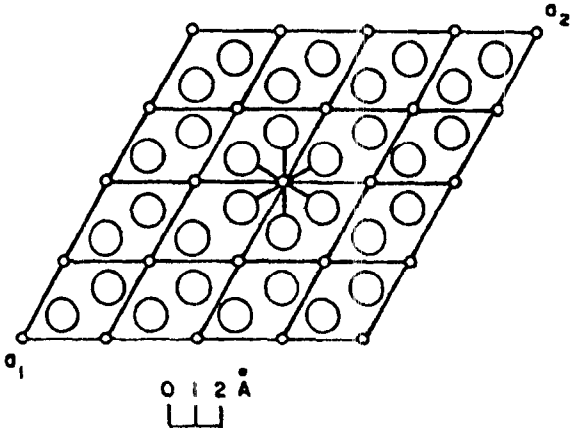

(a)

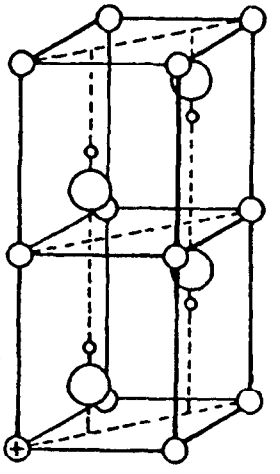

(b)

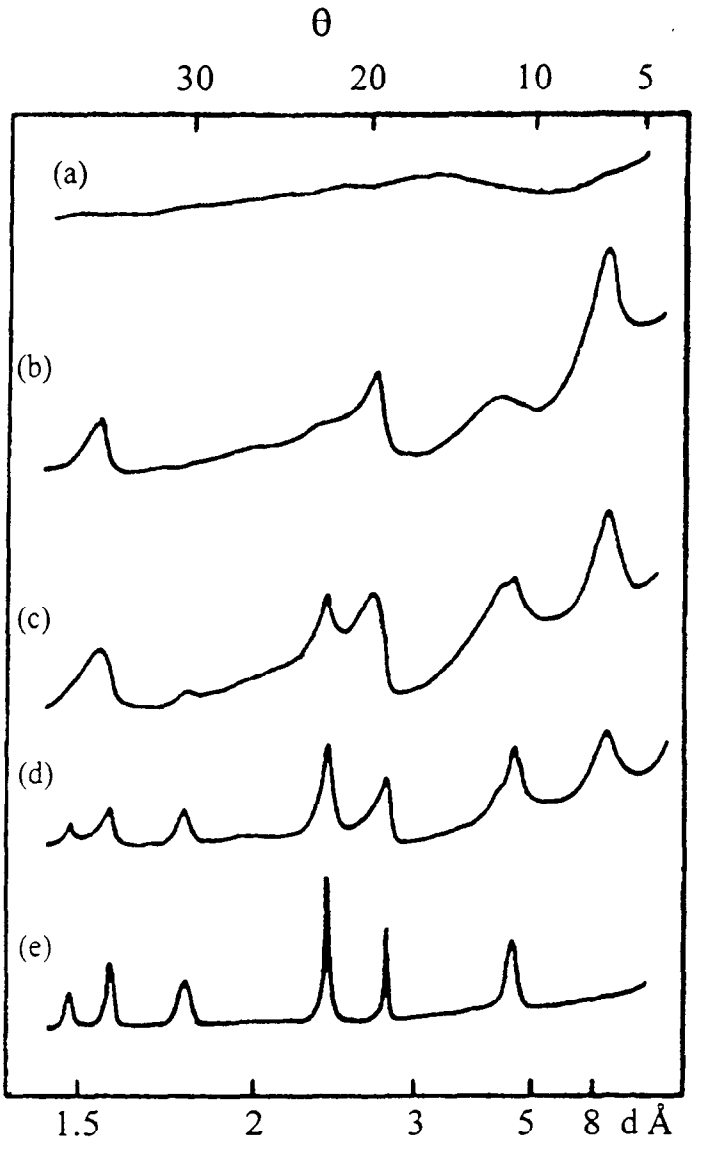
θ
30
20
10
5
(a)
(b)
(c)
(d)
(e)
1.5
2
3
5
8
d Å